WIND EXTRACTION FROM MULTIPLE METEOSAT CHANNELS

Henri LAURENT (*)

European Space Operation Centre
Robert-Bosch-Strasse 5
6100 Darmstadt, Germany

(*) Working under a EUMETSAT research fellowship

ABSTRACT

Satellite wind observations are operationally retrieved from cloud displacements in successive Meteosat infrared window images at ESOC. It is expected to obtain supplementary wind observations from each of the two other Meteosat channels : the water vapor absorption band channel and the visible channel.
A WV wind extraction algorithm has been running on the ESOC operational system in parallel to the operational IR wind scheme for several months. First statistics against radiosonde data suggest that the quality of the upper-level WV winds is as good as the quality of the upper-level IR winds, whereas the spatial coverage is larger. This is not true for medium-level winds.
The use of the VIS channel to compute cloud motion winds is also investigated. Preliminary results show the ability of the VIS cloud tracking to improve the number of lower level wind observations, and the potential of the high resolution VIS images compared to the infrared resolution.

1. INTRODUCTION

Winds measured by tracking cloud motions in successive satellite images are recognized as an important source of information for numerical weather prediction. Cloud-track winds are operationally retrieved at the European Space Operation Centre (ESOC) from the infrared window (IR : 10.5-12.5 μm) METEOSAT images. The scheme, described by Schmetz et al. (1992), uses a fully automatic cross-correlation method, human intervention being reduced to a final manual quality control. The basic area for the whole processing is an image segment, i.e. a 32x32 IR-pixel area (the IR pixel resolution is 5 km at the sub-satellite point). A multispectral image analysis, making use of the three channels, discriminates between the dominating scenes in an image segment, and provides information on potentially useful tracers for the cloud tracking.

Obviously the determination of winds fails in area without clouds. One possible extension of the cloud-track winds would be by tracking features in the water vapor absorption band channel available on METEOSAT (WV : 5.7-7.1 μm) , which would enhance the wind data in the middle and high troposphere (see e.g. Stewart et al., 1985). An automatic WV wind extraction scheme has been implemented at ESOC and is now running in parallel to the operational IR cloud-tracking scheme. First results on the WV wind quality are presented in section 2. A second possible extension of the current wind extraction scheme would be by cloud tracking in the METEOSAT visible channel (VIS : 0.4-1.1 μm) images, which could enhance the wind data in the low troposphere. Use of VIS images to compute cloud-track winds is being investigated at ESOC, preliminary results are presented in section 3.

2. WATER VAPOR WINDS

a) Methodology

The present operational satellite, since 21 June 1989, is METEOSAT-4. The WV data are available in eight bit resolution (instead of six bit for the previous METEOSAT satellites) every thirty minutes (instead of every hour). The signal to noise ratio in that channel is significantly higher, by a factor of two compared to METEOSAT-3 (Diekmann and Amans, 1990).

The computation of displacement vectors from successive WV images is similar to the computation of

cloud-track IR winds. The same cross-correlation algorithm is applied on original WV images, without any preprocessing. The automatic vector selection differs on two points : 1) as the surface is never sensed in the WV channel, there is no cloud-free area rejection, and 2) the temporal consistency check (also named symmetry test) is more stringent, in accordance with the less variable nature of the WV tracers.

The altitude assigned to the WV winds is the level where the atmospheric temperature reaches the brightness temperature of the tracked structures. Theses structures (high level clouds or pure water vapor structures) being colder than the background of the image segment, their radiance is estimated as the 20% smallest (i.e. coldest) WV radiances in the image segment. The brightness temperature is computed from this radiance through the Planck function and the radiometer filter function. The pressure level corresponding to that temperature is interpolated from the forecasts of the European Centre for Medium Range Weather Forecasts (ECMWF).

In the ESOC operational wind extraction chain, the automatically selected wind is compared with the collocated ECMWF wind forecast available, e.g. 24h forecast for the midday run, 12h or 36h forecast for the midnight run. At this stage, the drift wind is flagged if the norm of the vector difference with forecast wind is larger than 5 ms^{-1} and 0.55*Vf, where Vf is the forecast speed. This flag provides useful information but the final selection is performed during the manual quality control, when an experienced meteorologist takes the final decision on whether the vector is acceptable. For the WV winds the manual quality control was not performed.

b) Results

Figure 1 presents a part of the total WV wind field produced for 7 January 1991 at 1100 UTC, for upper levels (P <400 hPa). The IR wind field computed (before manual selection) for the same date and same area is presented on Fig. 2. Pressure levels assigned to the drift winds are also plotted in kPa, with a sign "-" when the drift wind does not agree with the collocated ECMWF forecast. WV winds are numerous and spatially consistent. When a high level cloud motion is tracked in the IR channel, the corresponding WV wind generally is also produced, and WV and IR winds are generally in very good agreement.

WV-track winds enlarge the area where IR cloud motion are tracked. Upper level WV-track winds which complement IR cloud-track winds often correspond to marginally cloudy areas, i.e. areas containing too small, too thin or too short-lived clouds to constitue valuables tracers for the IR tracking. Due to the WV continuity and to the background masking, such areas provide valuable WV structures to track. Furthermore, new motions are revealed by the WV tracking, in areas free of high-level IR tracers, for example over the Southern Atlantic. WV structures in the driest area appeared difficult to track and only a few mid-level vectors are produced (figure not shown). On average, about 90% of the total number of WV winds are assigned to levels above 400 hPa.

The present version of the WV wind scheme has been running twice a day, at 1100 and 2300 UTC since 11 April 1991. To assess their quality, WV winds are compared against radiosonde data. The statistical performance of the WV winds is compared with that of the operational IR winds, over a two month period, from 12 April 1991 until 11 June 1991. Two criteria are used to estimate the wind quality : the Root-Mean-Square (RMS) of the vector difference between the drift and the radiosonde wind, and the BIAS, defined as the mean of the norm difference, drift vector speed minus radiosonde wind speed. The operationally produced IR winds are systematically compared to collocated radiosonde winds, where the collocation area radius extends to 2° Latitude and within a one hour time interval. These statistics are performed for the disseminated winds, i.e. after the manual selection. For the WV winds, no manual selection was performed.

Table 1 shows the performance of the high-level drift winds. WV winds are more numerous by a factor of 2, which explains the larger number of collocations. The bias of WV and IR winds are nearly equal. RMS for WV winds (without manual selection) is slightly smaller than rms of IR winds (after manual selection). This result has to be moderated by taking into account the mean wind speed : for WV winds the mean speed of the collocated radiosondes was 19.7 ms^{-1}, whereas it was equal to 24.8 ms^{-1} for the

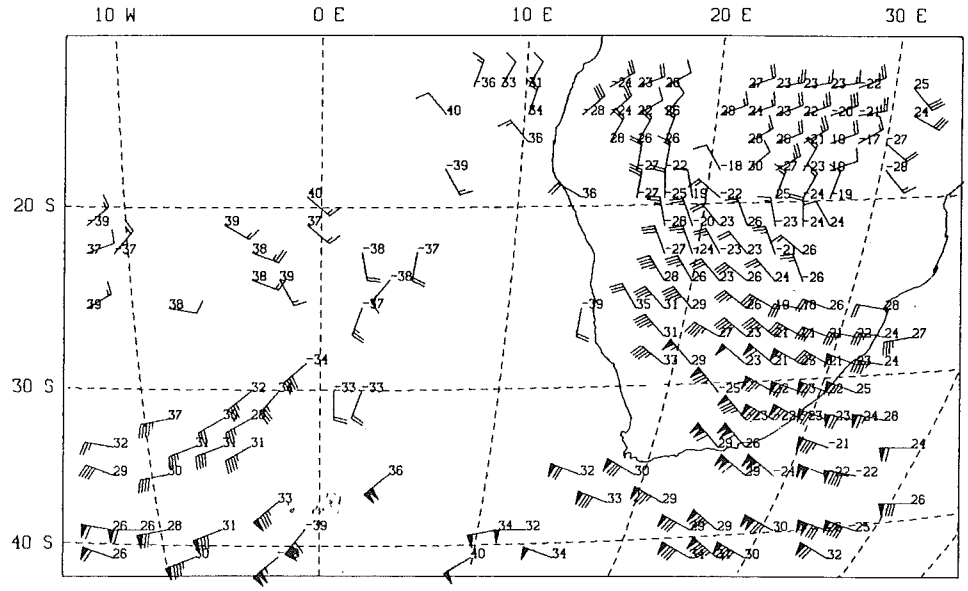

Figure 1. Upper level (p < 400 hPa) WV winds tracked at 1100 UTC 7 January 1991. Wind speeds are in knots.Associated presure levels are also plotted (kPa), a negative pressure indicating that the WV wind does not agree with the collocated ECMWF 24-h forecast.

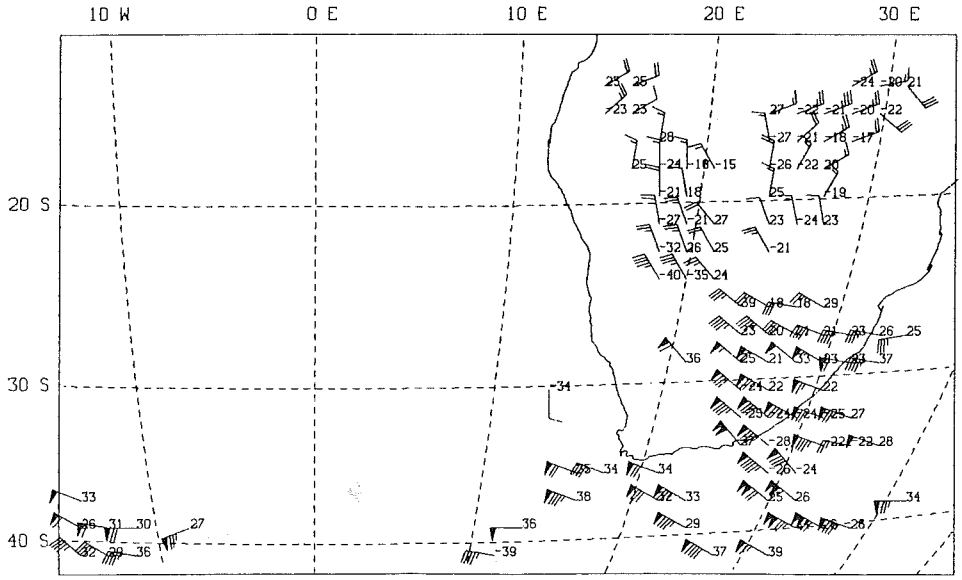

Figure 2. Same as Fig. 1, but for operational IR winds, before manual control.

HIGH LEVEL	WV WINDS	IR WINDS
Collocations	6776	1853
BIAS (m/s)	-1.0	-1.1
RMS (m/s)	9.2	9.5

Table 1. Retrieved high level (P < 400 hPa) winds compared with radiosonde

MID-LEVEL	WV WINDS	IR WINDS
Collocations	1241	2067
BIAS (m/s)	-3.5	-1.0
RMS (m/s)	10.7	7.1

Table 2. Same as Tab. 1, but for medium level (700 < P < 400 hPa).

IR winds. To compare the WV and IR winds, we have also examined the scores of the collocated winds, i.e. winds simultaneously produced in both channels at the same locations. For the sample of collocated WV and IR winds, the mean radiosonde wind speed was 23.7 ms^{-1}, the WV and IR mean scores were respectively -1.2 and -1.0 ms^{-1} for the bias, 6.7 and 6.9 ms^{-1} for the rms. The number of collocations with radiosonde was only 212, which is not enough to draw definite conclusions. As a tentative result it appears that the performances of the winds retrieved from the two channels are nearly equal.

The results for medium-level winds are presented in table 2. The WV wind bias and rms scores are worse than the IR wind scores at this level. It is not possible to guess what the WV wind scores would be if a manual quality control had been applied, nevertheless the ability of mid-level WV vectors to represent point winds as measured by radiosondes is questionable. In cloud-free regions the radiance reaching the satellite arises from a large layer of the middle troposphere, between about 300 and 550 hPa (Poc et al., 1980). A possible explanation for the strong negative bias is that the resulting WV-track vector can be a mixing of atmospheric winds at different levels, this averaged vector being on the whole smaller than single level wind vectors.

3. VISIBLE WINDS

A study on cloud motion wind extraction from METEOSAT VIS images was motivated by two main points. Firstly, low level clouds are often bright and better distinguishable in the VIS channel than in the IR channel where they poorly contrast with the surface. Secondly, the VIS channel spatial resolution is better, allowing the tracking of smaller structures.

a) Operational wind extraction scheme applied on VIS images

METEOSAT VIS images are available on full resolution (2.5 km at subsatellite point) or on the so-called "segmented" images which are sampled (every two lines and every two columns) from the full resolution to the IR resolution (5 km at subsatellite point). All the processing of the operational meteorological information extraction chain (e.g. cloud analysis, SST, IR winds, ...) is performed on the segmented images from the 3 channels.

The IR cloud-track scheme has been slightly modified to be applied on VIS segmented images. The computation is performed only if low level clouds exist in the segment, according to the results of the operational multispectral cloud analysis. Figure 3 displays an example of the low level ($p > 700$ hPa) cloud-track winds derived with the operational IR scheme, whereas Fig. 4 shows the vectors obtained using the corresponding VIS segmented images. The first obvious result of the VIS scheme is to improve the tracking of the stratocumulus (800-900 hPa) over the Southern Atlantic. In the IR channel the contrast between low level clouds and sea can be too small, then the tracking is difficult. In the VIS channel these clouds are very bright and well contrasted with the sea, hence the tracking is easy. But the usefulness of these additional winds is not obvious because a large number of IR winds are already retrieved in this area at low levels, with a good accuracy. It would probably be more useful to infer some low level winds over land, where almost none are produced at the moment. It is then encouraging to note that the westerly VIS vectors over land near 15S-20E (see Fig. 4) correspond to low level cloud motions, whereas high level clouds are tracked in this area with the IR channel (see Fig. 2). But the north-northwesterlies near 19S-22E result from high level cloud tracking. The improvement of the scheme will necessitate to improve the tracer identification.

b) Wind extraction from full resolution VIS images

The better spatial resolution of the VIS channel compared to that of the infrared channels seems potentially powerful for wind extraction. The size of the cross-correlation window for the IR and WV wind derivation is that of the segment, i.e. 32x32 IR-pixels, which corresponds to 64x64 VIS-pixels (full resolution). With VIS data smaller correlation windows can be chosen, with the aim to track low level cloud motions between high level clouds. Furthermore, the improved resolution of the general circulation

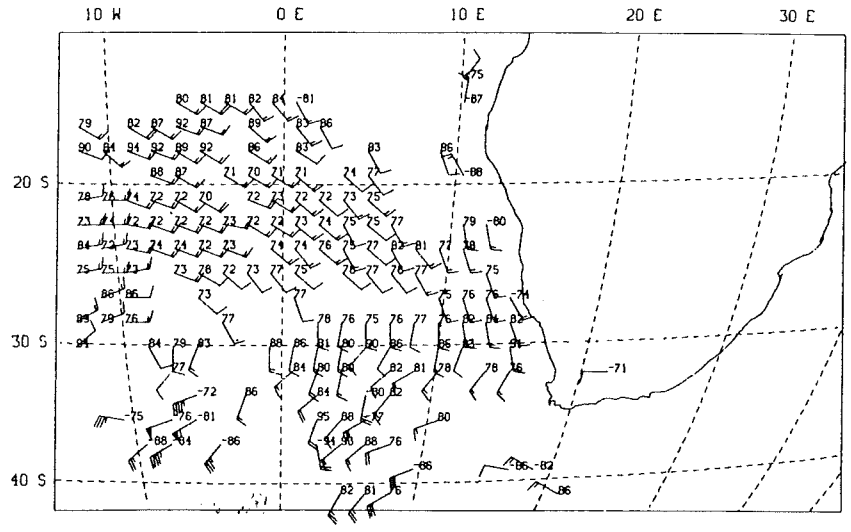

Figure 3. Same as Fig. 2, but for low-level (p > 700 hPa) IR winds.

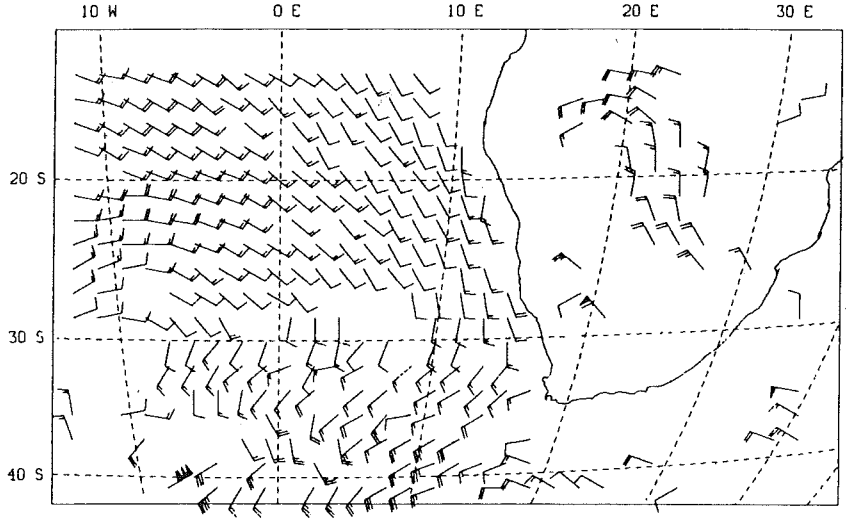

Figure 4. Cloud motion winds retrieved from segmented VIS images.

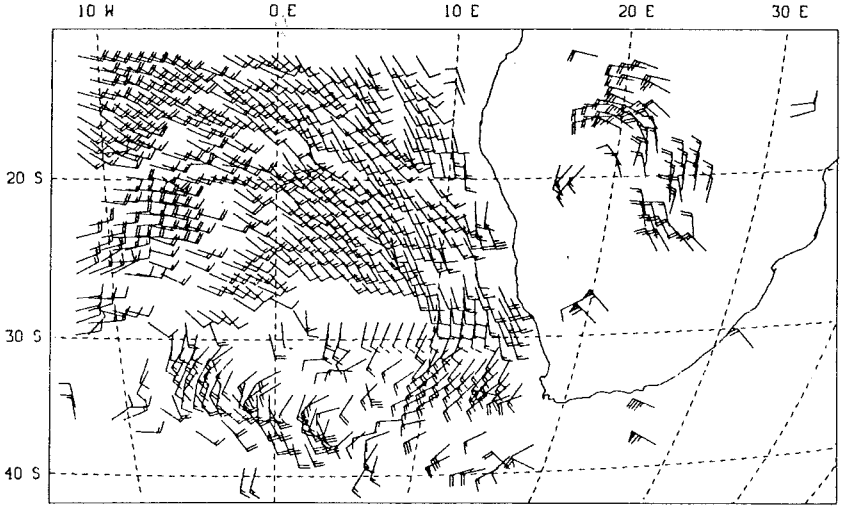

Figure 5. Cloud motion winds retrieved from full resolution VIS images, with a 32x32 correlation window.

DISPLACEMENT VECTORS FROM METEOSAT-WV-IMAGES USING A NEW EXTRACTION TECHNIQUE

G. Büche, A. Kummer, A. Ottenbacher and H. Fischer

Institut für Meteorologie und Klimaforschung
Kernforschungszentrum Karlsruhe/Universität Karlsruhe
Postfach 36 40
D-7500 Karlsruhe 1
Germany

ABSTRACT

The application of the cross correlation method to original water vapour images is becoming a standard technique in the evaluation of wind vectors for the middle troposphere. Nevertheless, the method fails in quite a lot of cases because of the smooth and shallow character of the grey value surface. It is shown that the results from correlation of original images can be approved and completed if pictures representing the derivatives like main curvatures or gradients of the originals are evaluated as well. As a consequence the number of acceptable displacement vectors can be increased by about 50 % if a small decrease of accuracy with respect to length and angle is tolerable.

INTRODUCTION

It has been shown by Kästner et al. (1980) and Eigenwillig and Fischer (1982) that water vapour images can be investigated sucessfully to evaluate wind vectors for the middle and upper troposphere. In the meantime the evaluation of water vapour wind vectors by application of the cross correlation method is becoming a standard technique. Details of this technique were published by Laurent et al. (1990) and Büche et al. (1990), where extended reference lists are given. Image sequences from the operational METEOSAT-4 are of clear nature and WV structures can be tracked immediately without preceeding image restoration. The method is compensated for the smooth and shallow character of WV structures by using a greater segment size of e.g. 48 x 48 pixels in the correlation technique compared to 32 x 32 pixels typically in operational cloud tracking from infrared image sequences (see Schmetz et al. 1987). Nevertheless the correlation technique fails in a lot of cases, where the grey value surface approaches the shape of a cylinder or even worse a plane resulting in unclear displacement signals at least in one coordinate direction.

The present paper concentrates on the evaluation of displacement vectors and shows that filter techniques can be advantageously used to increase the number of acceptable vectors. The scene of June 21, 1989, slots 23, 24 and 25 around 12 hours UTC has been selected by EUMETSAT for intercomparison purposes within the scope of a wind campaign. Corresponding segments of 1024 x 1024 pixels out of the WV image sequence are chosen for the analysis (Fig. 1). They cover South Europe and mainly West Africa and contain wide areas with pure water vapour emission as well as others where signals con-

Fig.1 Water vapour channel scene taken by METEOSAT-4 on 21 June 1989 over West Africa and South Europe.

tain information from clouds. The main features are the inner tropical convergence zone in the lower part of the image, a jet stream flowing from the Gulf of Guinea to Libya (approximately the diagonal from lower left to upper right) and cloud fields from the Azores to Europe (upper left part).

METHOD

Reference set of displacement vectors

Throughout this work the conventional cross correlation method is applied using a segment size of $N^2 = 48 \times 48$ pixels. This number is taken over from our earlier work as a good compromise both with respect to stabil-

ity and uniqueness of the method as well as computer time needed for the evaluation. The step size between neighbouring segments is taken equal to N in order to guarantee that resulting displacement vectors are really independent and free of interpolation effects. Then twice a total of 19 x 19 displacement vectors results from a time sequence of 3 images A, B and C using the given numbers for the sizes of images, segments and steps.

In order to evaluate a figure of merit for displacement vectors from filtered images a representative set of vector pairs from original images is needed. First the lenghts of vectors evaluated from images A and B are compared to those obtained from B and C. From Fig. 2 it is evident that a relative difference of length

$$|\Delta L| = 2 \cdot \frac{||BC| - |AB||}{|BC| + |AB|} \qquad (1)$$

smaller or equal to 40 % excludes cases where one of the vectors approaches zero length or is unreasonably long. From Fig. 3 it is concluded that angles between corresponding vectors should not exceed 30 degrees. In addition to that, all lengths should

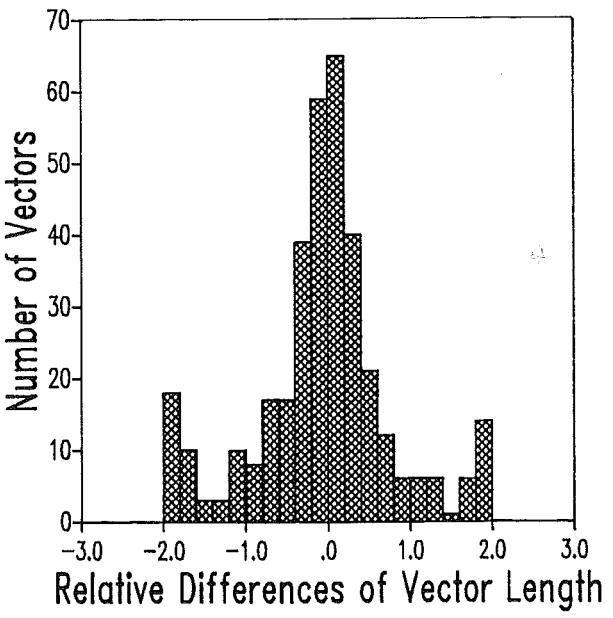

Fig.2 The number of displacement vector pairs evaluated from 3 original images plotted over their relative differences of the length ΔL.

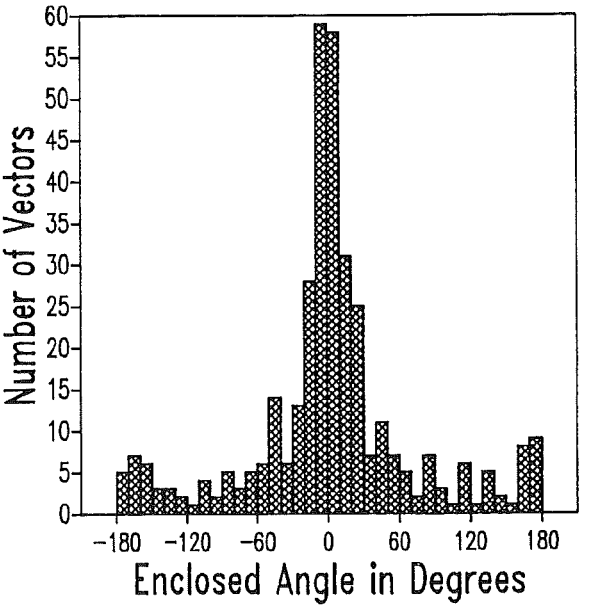

Fig.3 The number of displacement vector pairs as a function of enclosed angle.

be greater than zero. The set of remaining vector pairs is defined to be a "good" one, i.e. it guarantees that grey value structures within segments are clearly shaped and do not change too much in time. The number of pairs found is 152 (out of 361), their root mean square (r.m.s.) deviation of vector length is ± 19 % (compared to ±83 % for all pairs) and the r.m.s. deviation of angle is ± 14° (± 71° for all). In both cases the mean values are very close to zero. These numbers cannot be lowered essentially and should be taken as inherently connected with the selected scenes.

Effect of median filters

To show the effect of filters on the number of good vectors a series of homogeneous median filters is applied to original images with n times n elements as a parameter. The values of the standard deviations for length difference and enclosed angle between vectors from filtered (AB_F; BC_F) and corresponding original images ($AB_{Orig.}$; $BC_{Orig.}$) are plotted in Fig. 4. Both become greater with in-

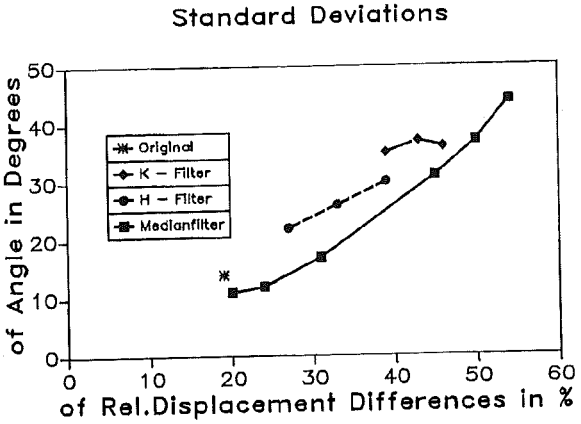

Fig. 4 Standard deviations of relative displacement vector differences and enclosed angle for results from filtered images compared to those from the originals. The numbers are a function of the filter size n and are to be added quadratically to those inherent to the original images.

creasing n and show the loss of information introduced by the averaging process. After an initial increase the number of "good" vectors (as defined above) that are obtained from filtered images decreases as expected. But the number of additional good vectors, i.e. results from filtered images at places where no acceptable result exists from the original remains almost constant (see Fig. 5). Consequently, the application of a small filter mask results in roughly 33 % more good displacement vectors but on the cost of a reduced accuracy in length ($\geq$ 20 %) and angle ($\geq$ 12°).

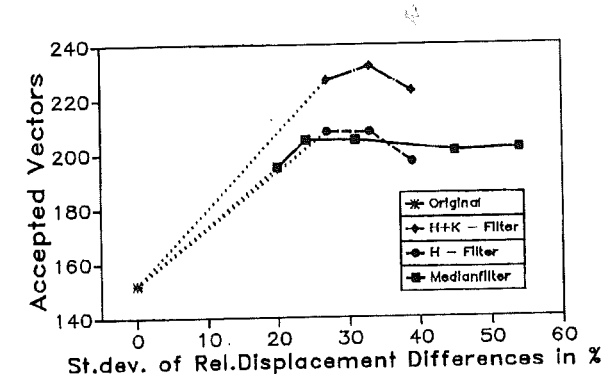

Fig. 5 The number of good vector pairs if those from filtered images are accepted at places where no good results from original images exist.

MORE SOPHISTICATED FILTERS

The filters to be discussed in this chapter are essentially of different kind and can be applied in pairs. They estimate the first and second order derivatives of the grey values surface and combine them in specific ways. The information content of the original image is split into two linearly independent subsets which allow for reconstruction of the original up to the first or second order, respectively. A certain smoothing effect is included in the transformation process. The free parameters are: the grid size n for the estimation of derivatives using the method of differences; the grid size and the parameter σ when Gaussian differential operators are applied.

The pair of filters H and K calculates pixel by pixel the main curvatures κ_1 and κ_2 of the surface from the surroundings and combines them to the average ($H = (\kappa_1 + \kappa_2)/2$) and Gaussian ($K = \kappa_1 \kappa_2$) curvatures. The resulting two images look quite different from the original but their structures show equivalent displacements (Büche et al. 1990). The standard deviations for the relative differences of vector lengths and for the angles between the vectors obtained from corresponding sites within transformed and original images are plotted in Fig. 4 as well. The uncertainty introduced from H-filtering is not too far off from the effect of homogeneous median filters using the same grid size. But the K -transformation is more sensitive to variations of grey values resulting in somewhat increased length and angle uncertainties. However, their main advantage is linear independence and the results can be combined. The number of good vector pairs from the originals is increased by about 37 % if those from H-transformed ones are included. This number even rises to 53 % if good results from K-transformed images are added as well after the inclusion of those from H-transformed ones (see Fig. 5).

During the application of the following pair of filters the absolute value and angle of the gradient (hereafter called G and P, respectively) are calculated from the surroundings of each pixel (Korn, 1988). Like H the trans-

formation G has a certain smoothing effect. But the direction P of the gradient is even more sensitive to variations of grey values than the Gaussian curvature K. The related numbers for the uncertainties of displacement vector length and enclosed angle are given in Fig. 6 where results from Gaussian

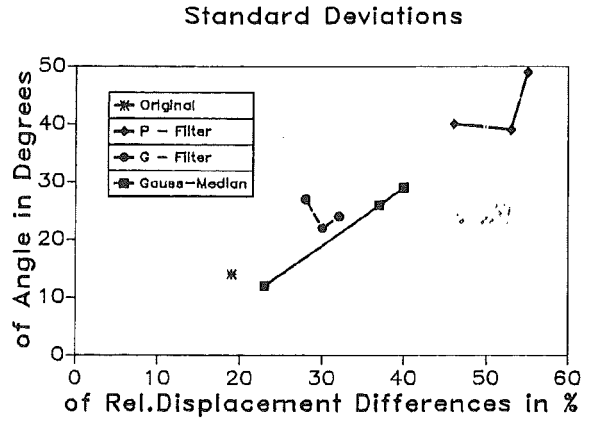

Fig. 6 Standard deviations of relative displacement vector differences and enclosed angle for results from filtered images compared to those from the originals.

median filtering with the corresponding parameters are included. The curves for G and P show greater mutual distance than those found from H and K-transformations. The corresponding numbers for the additional good vector pairs are 35 % (for G) and 48 % (for G and then P, successively; see Fig. 7).

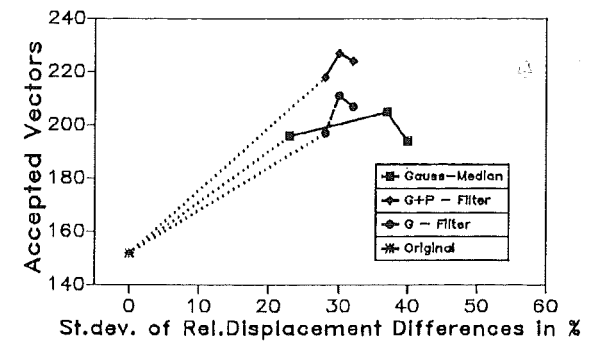

Fig. 7 The number of good vector pairs if those from filtered images are accepted at places where no good results from original images exist.

CONCLUSIONS

It is shown that filters can successfully be used to increase the number of acceptable vector pairs from structure tracking within water vapour images. For all cases considered in this paper the filtering process conserves the length and direction of displacement vectors on average, but the related standard deviations increase with increasing information loss. Even weak median filtering with homogeneous weights increases the number of acceptable displacement vectors considerably. However, this gain is still enhanced by the application of filter pairs. The results can be added in successive order according to the levels of uncertainty in length and angle (Fig. 8). Finally, the number of accepted vectors is increased by about 50 % on the cost of an additional uncertainty which does not go far beyond that one inherently connected with the imaging and evaluation techniques. Many of these additional vector pairs are found close to or within smooth regions of the grey values surface which appeared to be problematic for structure tracking from originals.

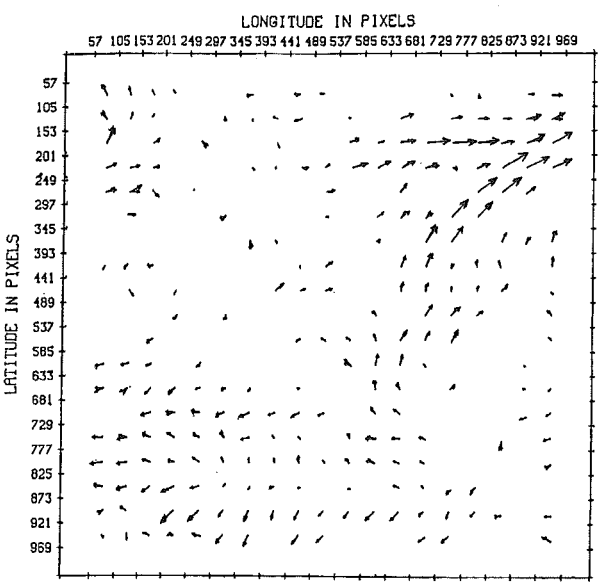

Fig. 8 Field of displacement vectors deduced from a sequence of 3 water vapour images as shown in Fig 1. Results from H- and K-transformed images are included.

ACKNOWLEDGEMENTS

The authors are indebted to EUMETSAT for supplying the METEOSAT images free of charge within the scope of a wind campaign initiated by Deutscher Wetterdienst. We thank Mrs. S. Honçu for her patient help in questions of programming. The competent assistance from members of the KfK computer center and of the reprographic service is gratefully acknowledged.

REFERENCES

BÜCHE, G., Ottenbacher, A. and Fischer, H., (1990) "Wind vectors evaluated from structures within consecutive METEOSAT water vapour images". Proceedings of the XXVIII Plenary Meeting of COSPAR, The Hague, 25th June - 6th July 1990, (in press).

BÜCHE, G., Ottenbacher, A. and Fischer, H., (1990) "Wind vectors evaluated from structures within consecutive METEOSAT water vapour images". Proceedings of the 8th METEOSAT Scientific Users' Meeting, Norrköping, Sweden, 28th - 31st August 1990, pp. 87 - 96.

EIGENWILLIG, N. and Fischer, H.,(1982) "Determination of midtropospheric wind vectors by tracking pure water vapor structures in METEOSAT water vapor image sequences." Bull. Americ. Meteor. Soc. 63, pp. 44 - 58.

KÄSTNER, M., Fischer, H. and Bolle, H.J. (1980) "Wind determination from NIMBUS 5 observations in the 6.3 µm water vapour band". J. Appl. Meteor., 19, pp. 409 - 418.

KORN, A., (1988) " Toward a symbolic representation of intensity changes in images". IEEE Transactions on Pattern Analysis and Machine Intelligence, 10, pp. 610 - 625.

LAURENT, H. and Desbois, M. (1990) "Measurement and validation of atmospheric motions detected on water vapour METEOSAT imagery". Proceedings of the XXVIII Plenary Meeting of COSPAR, The Hague, 25th June - 6th July 1990, (in press).

LAURENT, H. (1990) "Feasibility study on water vapour wind extraction techniques". Report from the Laboratoire de Météorologie Dynamique du CRNS, Ecole Polytechnique, F-91128 Palaiseau, France, 80 pp.

SCHMETZ, J. and Nuret, M. (1987) "Automatic tracking of high-level clouds in METEOSAT infrared images with a radiance windowing technique". ESA Journal, 11, pp. 275 - 286.